Time-resolved plasma spectroscopy of thin foils heated by a relativistic-intensity short-pulse laser

P. Audebert,[1] R. Shepherd,[2] K. B. Fournier,[2] O. Peyrusse,[3] D. Price,[2] R. W. Lee,[2] P. Springer,[2] J.-C. Gauthier,[1] and L. Klein[4]

[1]*Laboratoire pour l'Utilisation des Lasers Intenses, UMR 7605, CNRS-CEA-Université Paris VI-École Polytechnique, 91128 Palaiseau, France*

[2]*Lawrence Livermore National Laboratory, University of California, Livermore, California 94550*

[3]*Commissariat à l'Énergie Atomique, Boîte Postale 12, 91680 Bruyères-le-Châtel, France*

[4]*Department of Physics and Astronomy, Howard University, Washington, Washington, DC 20059*

(Received 31 May 2002; published 19 December 2002)

Time-resolved *K*-shell x-ray spectra are recorded from sub-100 nm aluminum foils irradiated by 150-fs laser pulses at relativistic intensities of $I\lambda^2 = 2\times 10^{18}$ W μm^2/cm^2. The thermal penetration depth is greater than the foil thickness in these targets so that uniform heating takes place at constant density before hydrodynamic motion occurs. The high-contrast, high-intensity laser pulse, broad spectral band, and short time resolution utilized in this experiment permit a simplified interpretation of the dynamical evolution of the radiating matter. The observed spectrum displays two distinct phases. At early time, $\leqslant$500 fs after detecting target emission, a broad quasicontinuous spectral feature with strong satellite emission from multiply excited levels is seen. At a later time, the He-like resonance line emission is dominant. The time-integrated data is in accord with previous studies with time resolution greater than 1 ps. The early time satellite emission is shown to be a signature of an initial large area, high density, low-temperature plasma created in the foil by fast electrons accelerated by the intense radiation field in the laser spot. We conclude that, because of this early time phenomenon and contrary to previous predictions, a short, high-intensity laser pulse incident on a thin foil does not create a uniform hot and dense plasma. The heating mechanism has been studied as a function of foil thickness, laser pulse length, and intensity. In addition, the spectra are found to be in broad agreement with a hydrodynamic expansion code postprocessed by a collisional-radiative model based on superconfiguration average rates and on the unresolved transition array formalism.

DOI: 10.1103/PhysRevE.66.066412 PACS number(s): 52.50.Jm, 52.70.La

I. INTRODUCTION

In recent years, the technology of ultrashort laser pulse generation has progressed to the point that 100-fs optical pulses, amplified to energies of a few hundred millijoules, corresponding to focused intensities exceeding 10^{18} W/cm^2, are routinely produced. Such intensities can be used to heat solid materials to elevated temperatures with minimal hydrodynamic expansion, producing an extremely high energy density state of matter for a short period of time [1]. Because of the extreme conditions reached, studies of this type are of fundamental interest to laboratory astrophysical investigations in addition to the obvious significance these plasmas have for research on bright x-ray sources. The experiment presented here employs improved instrumentation that permits a measurement of the time evolution of the plasma heating that extends and sometimes contradicts previous ideas on the mechanisms involved. The principal experimental enhancements lie in the use of shorter time resolution (500 fs), larger crystal x-ray spectrometer energy range (400 eV), better control and management of the laser pulse energy contrast, and higher, relativistic, laser intensity ($\geqslant 10^{19}$ W/cm^2). The higher intensity used in this experiment is required to obtain sufficient radiated energy to permit detection over the wider energy range used here. Taken together these permit a much better picture of the evolution of the laser plasma interaction.

Many groups have recorded x-ray spectra emitted from solid targets heated with an ultrashort laser pulse [2–9]. Typically, these experiments have been performed with the laser light focused on a thick solid target. With a pulse showing a high intensity contrast between the pedestal and the peak, inverse bremsstrahlung heats the first tens of nanometers—several skin depths—of the overdense interaction region, while high energy electrons, produced by resonance absorption, heat the solid matter deep inside the target. These effects are amplified by the use of *P* polarization, which favors resonance absorption and increases the hot electron population. The suprathermal electrons deposit their energy far from the laser focal spot [10,11], so that large scale length longitudinal and radial spatial gradients are produced in these thick targets. Because of the temperature and density gradients, the resulting x-ray emission from this plasma with extreme temporal dynamics is very difficult to interpret. Finally, although some of these previous experiments have used fast x-ray streak cameras to time resolve ($\sim$1 ps) the x-ray emission [12–14], most experiments have been performed with time-integrated x-ray diagnostics.

In this paper we extend and refine these previous studies through a detailed spectroscopic analysis of the subpicosecond dynamics of the *K*-shell emission from ultrathin aluminum foils heated with a high-intensity, high contrast, ultrashort-pulse laser. The small thickness of the foils ($<$100 nm) was chosen to minimize the uncertainty in one dimension in the heating and cooling rates due to heat conduction [13,15]. Indeed, with foil thickness much smaller than the thermal penetration depth [15], the entire target should be heated uniformly at constant density if electron

conduction can propagate the laser heating over the foil thickness before significant hydrodynamic motion occurs. The spectral region that includes the He-like transitions $1s^2$-$1s2p$, He_α, $1s^2$-$1s3p$ He_β, and $1s^2$-$1s4p$, He_γ and the associated satellite line transitions was recorded using a time-resolved crystal spectrograph. The experimental spectrum recorded in the first 500 fs after detecting target emission is dramatically different from that recorded in previous experiments. In this initial time, unexpectedly strong emission of a broad satellite spectrum is observed. In the next 500 fs, He-like resonance line emission begins to increase relative to the satellite emission, and the spectrum integrated over several picoseconds is dominated by line emission, becoming the same as that observed in the previous studies cited above.

We interpret the spectral data with a simple atomic physics model that compares the number and volume of the ions that emit resonance lines to the number and volume of those emitting the associated satellites. This model leads to the conclusion that the heating, although uniform in the longitudinal direction, is not uniform over the transverse area of the foil. In fact, there appears to be a heating mechanism that results in two different spatial plasmas. Initially, during the laser pulse, fast electrons, produced by intense laser field acceleration in the laser spot and an associated return current, heat an extended volume of the foil. After the pulse, the hot electrons rapidly thermalize (100 fs time scale) and the plasma in the extended volume relaxes to a uniform low temperature plasma of several hundred eV. The associated production of ions with multiply excited levels in this extended volume results in the observed satellite emission. The laser spot attains a temperature of several keV during the laser pulse, and emits primarily He-like resonance lines. Following the first 500 fs after detecting target emission, cooling by expansion becomes important, the satellite emission weakens, and the emission of resonance lines from the hot laser spot dominates. The duration of the spectral line emission was found to be on the order of 2 ps, the same as that observed in earlier studies, but with the difference that the resonance lines appear later in the foil heating phase than was supposed previously. To obtain more detailed dynamic information, the spectra recorded in this experiment were also compared to simple hydrodynamic simulations involving level populations, line intensities, and spectral shapes calculated by a collisional-radiative model [16] using the superconfiguration approximation [17]. The plasma parameters were varied until the linewidths, peaks, and shapes matched the data for all times, producing a reasonable estimate of the temporal evolution of the plasma conditions.

Previous studies, based on spectral diagnostics with picosecond or greater time resolution, yield a spectrum equivalent to the time-integrated result of this experiment and therefore, do not contain information on the dynamical evolution of the plasma. For this reason, some of the previous investigations have led to erroneous conclusions about a two-temperature distribution in the laser spot. Especially significant is our conclusion that a high intensity, short laser pulse incident on a thin foil cannot create a uniform hot and dense plasma. This is because, at high intensity (even with a high contrast laser pulse), most of the energy in the laser spot is converted into fast electrons that heat the target bulk laterally beyond the laser spot. The early time satellite emission we observe is the signature of a high density low temperature plasma. This spectrum is overwhelmed at a later time by the line emission that was seen in previous experiments. For our targets, therefore, the initial laser created plasma has a very low temperature in a large area surrounding the hot laser spot, emitting a satellite spectrum that at a later time is dominated by the line emission from the smaller hotter laser-spot plasma.

The paper is organized as follows: In Sec. II we describe the instrumentation and experimental setup, in Sec. III we present the spectral data, which is analyzed in Sec. IV; and in Sec. V we present a summary and conclusions.

II. EXPERIMENT

The experiments were performed at the Lawrence Livermore National Laboratory ultra short-pulse laser facility. The laser has been described in detail elsewhere [18], so only a brief description will be given here. The laser utilizes chirped pulse amplification to generate high energy, 150-fs-duration pulses. The pulses from an 82-MHz Ti:sapphire oscillator are temporally stretched and amplified in three stages: a regenerative amplifier, followed by a five-pass power amplifier, and finally a large aperture two-pass power amplifier. The pulses are compressed in a vacuum compressor, frequency doubled with a 1.5-mm-thick potassium dihydrogen phosphate (KD*P) crystal, and focused on a target with an $f/3.5$ off-axis parabola. The energy on the target is measured to be from 150 to 200 mJ at 400 nm wavelength and can be focused to a full-width at half-maximum (FWHM) spot size of 2 μm. Equivalent plane images indicate that 53% of the laser energy was located in the $1/e^2$ central spot.

A significant effort was made in the experiment to suppress any prepulse or pedestal and to insure high contrast, high-intensity pulses. The laser output pulse duration was monitored on a shot-to-shot basis, by imaging the zero-order reflection from the compressor grating into a spectrometer. To minimize the probability of a pulse with temporal ''wings'' being used in the experiment, pulses deviating more than 10% from the initial 100-fs Gaussian pulse were shuttered and prevented from further amplification. The phase of the pulse also was monitored on a shot-to-shot basis with a frequency resolved optical gate system [19], so that data from poorly compressed pulses could be rejected. The level of amplified spontaneous emission (ASE) is also of critical concern in laser ultrathin foil interaction, since focused ASE can cause target expansion before the ultrashort pulse heating occurs. To suppress ASE, the laser pulse was frequency doubled with a 1.5-mm-thick KD*P crystal. Distortions in the time and space profiles of the pulse introduced by the frequency doubling were controlled by measuring the spectrum and energy of the frequency-doubled laser light, and adjusting the energy until an undistorted frequency spectrum was produced. A high-dynamic range, third-order, scanning autocorrelation measurement was performed on the 800-nm pulse, with results indicating that the fundamental frequency

pulse had an intensity contrast of $I_{\text{background}}/I_{\text{peak}} \approx 10^{-5}$ at 1.5 ps before the peak of the laser pulse. This level of contrast is further enhanced (approximately squared) by frequency doubling. A low-dynamic range (10^{-4}), single shot autocorrelation was performed on every shot and used to monitor the pulse width, while a calorimeter was used to measure the energy on target. To check for any ASE effect, the unseeded pulse was focused on the 25-nm foil target and no damage was observed, suggesting that no measurable effect exists. The contrast between the pulse and prepulses, due to leakage of the regenerative amplifier, was also measured and found to be below 10^{12}. As an additional check of the temporal contrast, an energy monitor was placed behind the targets during the shots and no transmitted energy was detected through the foils. Because of all the precautions taken in this experiment to insure the suppression of pulse pedestals, we believe that the plasma density scale length is that defined by the expansion of the plasma due to the heating of the 100-fs laser pulse.

To minimize resonance absorption and hence reduce the production of fast electrons, the experiments were conducted with *S*-polarized light. A 22.5° angle of incidence (relative to target normal) was chosen in order to collect specular light for alignment and to protect the laser chain. A peak laser intensity of 10^{19} W/cm^2 ($I\lambda^2 \approx 2\times 10^{18}\ W\,\mu\text{m}^2/\text{cm}^2$) was used. The pulse duration could be varied from 150 fs to 1 ps by increasing the distance between the two gratings of the compressor. The increased pulse duration reduced the maximum focused laser intensity to about 10^{18} W/cm^2. In addition, the focal spot size could be increased by inserting a variable diameter aperture in the beam path, resulting in an increase in the *f* number of the off-axis parabola. The increased spot size faciltes the study of targets irradiated with laser pulses at irradiances between 10^{17} W/cm^2 and 10^{19} W/cm^2.

The emitted x-rays were collected with a 500 fs time-resolution streak camera interfaced to a dual-crystal Von Hamòs [20] x-ray spectrograph, schematically illustrated in Fig. 1. The streak camera was small enough to fit inside the vacuum chamber, allowing the entrance slit to lie along the focusing axis of the crystals. The dual-crystal design allowed simultaneous collection of time-resolved data from multiple He-like spectral lines. Two RbAP crystals were bent to 3.6 and 3.0 cm radii to collect time-resolved data from the He_α transition and the He_β and He_γ transitions, respectively. The spectral data were focused onto the 25.4-mm long, 150-μm wide entrance slit of the streak camera. Because of the high streak camera sweep speed (2.6 ps/mm), the transit time difference for x-rays reflecting off the two crystals produced a spatial gap between the streaked data from the respective crystals. The transit time difference of the x-rays at different wavelengths, reflected off a single crystal, was used to calibrate and check the linearity of the sweep for each shot. The streaked data were intensified and collected with an image intensifier mated to a 1024×1024 charge-coupled device (CCD) camera. The x-rays emitted with energies between 10 keV and 1 MeV were characterized using a scintillator (diode) array. Eight filtered NaI scintillators coupled to photomultipliers were used for detection above 30 keV, and three

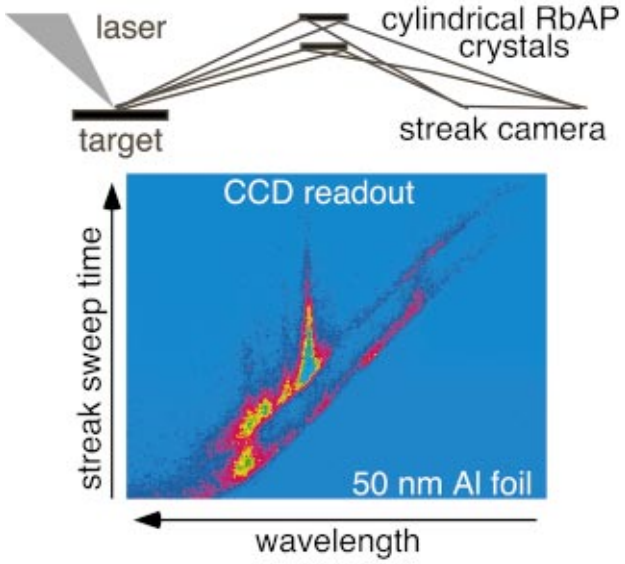

FIG. 1. (Color) Experimental setup of the laser focusing and dual-crystal x-ray collection. Typical data obtained for a 2×10^{19} W/cm^2, 150-fs pulse incident on a 50-nm Al foil. The upper trace shows the He_α line transition and Li-like dielectronic satellites. The lower trace shows the He_β and He_γ line transitions.

filtered x-ray diodes were used for detection below that energy. The thicknesses of the scintillators and of the filters (Al+Pb) were chosen to ensure that the x-ray spectra could be reconstructed from their output. The spectra were found to resemble a Maxwellian that could be fitted with a single temperature with good reproducibility. The temperatures were found to be between 120 and 200 keV, depending on the laser energy. Finally, no spatial information was available from the streak camera record as the spatial resolution of the streak camera is larger than the focal spot.

To examine the effect of target size, three free-standing aluminum target thicknesses—25 nm, 50 nm, and 75 nm—were used. Each foil was suspended over an array of 1.7-mm-diameter holes in a ceramic substrate. The 1.7 mm diameter foil area was destroyed and replaced after each shot. In Fig. 1 the data for the case of a 150-fs, 2×10^{19}-W/cm^2 laser pulse incident on a 50-nm-thick Al foil target is displayed as a function of the streak camera sweep time. The transit time difference for x-rays reflecting off the two crystals is responsible for the spatial gap between the streaked data in the two frequency ranges. Both traces are inclined because of the time delay due to the path difference between low and high energy photons.

III. SPECTRAL DATA

The intensity data of Fig. 1 are presented again in Fig. 2 in a plot of x-ray wavelength vs target arrival time. The spectra are corrected for streak camera CsI photocathode response, image intensifier gain, different solid angles of the crystal x-ray reflection, and time difference related to the different path lengths. All the traces analyzed in the following have these corrections applied to the raw data. The positions of the He-like resonance lines and their associated Li-,

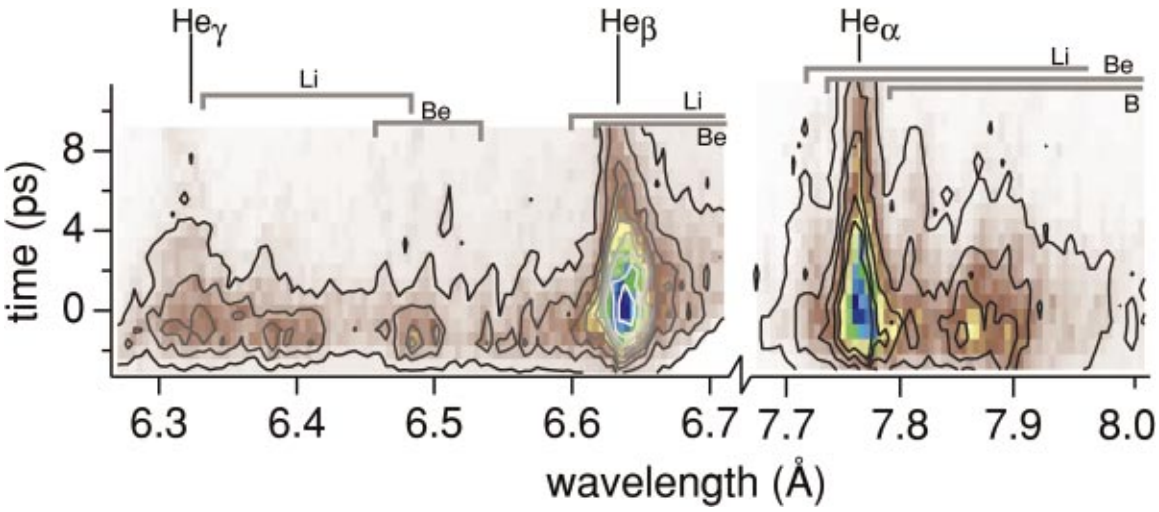

FIG. 2. (Color) Time-resolved data for the same conditions as Fig. 1. The time axis is that of the x-ray arrival time at the target. The entire spectrum from He_γ (6.314 Å) to He_α (7.757 Å) is displayed in one data record.

Be-, and B-like satellites have been identified in the figure.

Several traces of the time-resolved data of Fig. 2 over the spectral range from He_β to He_γ are presented in Fig. 3. The spectrum is displayed both at early time and at the time of peak emission with the same intensity scale. The background due to noise is indicated to demonstrate that the early time spectrum is in fact Al emission and the time-integrated data is presented for a final comparison. The initial spectrum is recorded over the first 500 fs, starting at the time when emission exceeded the background and the peak emission data is taken 3 ps later. It is to be emphasized that the features observed in the initial spectrum are reproducible and are well above the background noise level. It is important to note that the integrated intensity of the initial emission in the spectral region between 6.35 and 6.55 Å is comparable to the integrated intensity of the initial resonance lines (≈ 0.2 of He_β). This strong emission between the two He lines has been found, see Sec. IV below, to originate from doubly excited

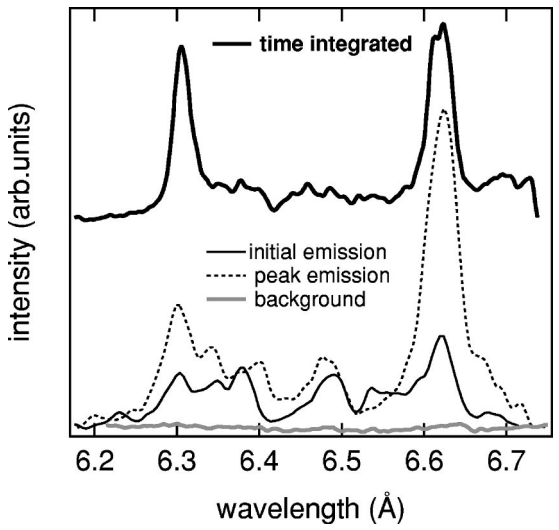

FIG. 3. Spectral traces of Fig. 2 data in the region from He_γ to He_β (see text).

$1s2l4l'$ levels [13,21]. At the initiation of the emission, He_β and He_γ appear as broad features and only later emerge as the narrow lines seen in the peak emission and time integrated data.

In Fig. 4 we again omit the He_α spectra to simplify the display of the data and present the reduced He_β and He_γ spectra for the 25 nm, 50 nm, and 75 nm foils irradiated at 2×10^{19} W/cm^2. Results for two heating pulse durations of 150 fs and 1 ps are shown. In addition to the corrections described above, the spectra from the three target thicknesses have been adjusted to account for the different number of emitters. This emitter-number scaling is convenient as it results in the same order of magnitude for the x-ray intensities of all six spectra. Note that as in Fig. 3, the resonance lines He_β and He_γ barely emerge from an intense continuum during the rising edge of the laser pulse, become very broad at the peak of the laser pulse, and narrow at much later times. Previous experimental emission spectra of similar near-solid density, sub-100-nm foils, with picosecond time resolution can be found, for example, in Refs. [14,22], and are in agreement with the time-integrated spectrum of Fig. 3. An important observation from the present experiment is that the time duration of the He_β and He_γ lines is shorter as the foil thickness increases, for both laser pulse widths. Note also that the strong satellite emission between these two lines that originates from doubly excited $1s2l4l'$ levels [21] decreases with foil thickness. When increasing the laser pulse width from 150 fs to 1 ps, the emission duration of the He_β and He_γ resonance lines also increases. Furthermore, the intensity of the satellite emission relative to the He_β and He_γ resonance line intensities seems to be independent of the laser irradiance, even when the laser intensity is decreased by two orders of magnitude.

The He_α line, near 7.757 Å, also exhibits strong satellite emission. Several groups of Li-like satellites appear on the long wavelength (red) side of He_α. Similar to the satellites observed between He_β and He_γ, the red satellite emission increases in intensity as the foil thickness is increased. In

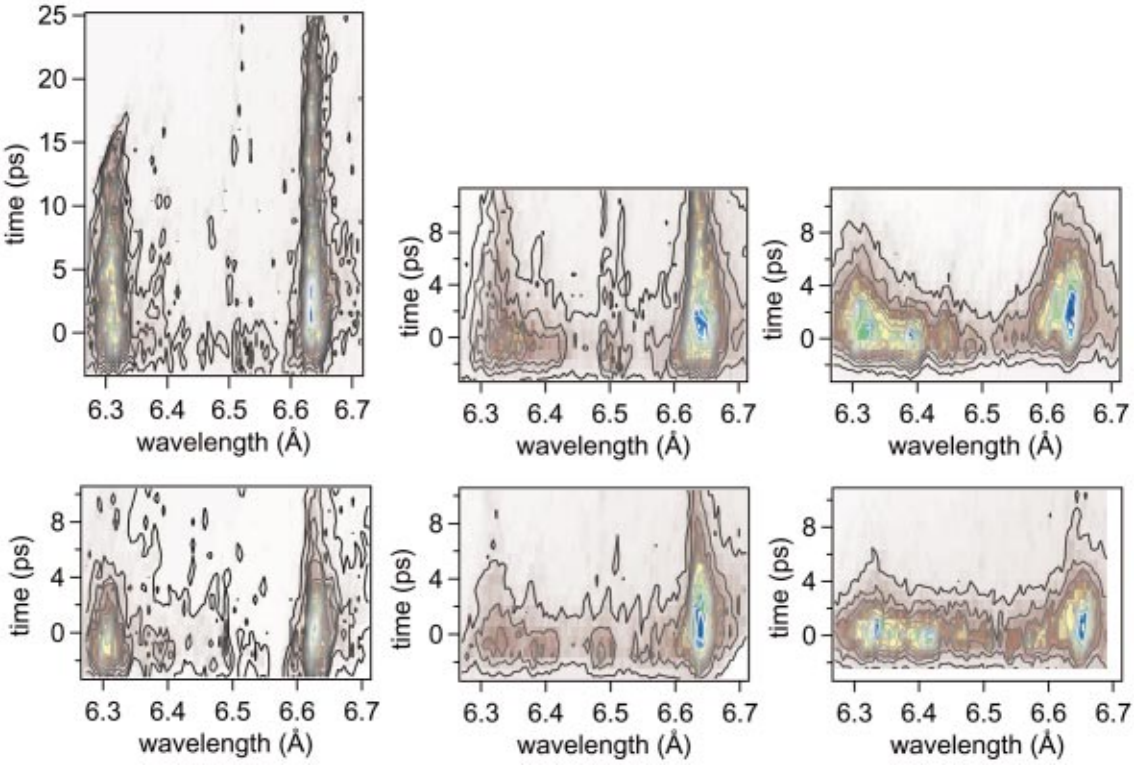

FIG. 4. (Color) Time-resolved data for the spectral range covering the region from He_γ (6.314 Å) to He_β (6.635 Å) line transitions. The upper (lower) series corresponds to a laser pulse duration of 1 ps (150 fs). Left, 25 nm; center, 50 nm; right, 75 nm. The time origin coincides with the peak of the laser pulse.

addition, an extended wing appears on the short wavelength (blue) side of the resonance line. This blue wing is strongly apparent at the peak of the laser pulse, but changes into a blue satellite line at later times. Recently, this blue satellite line has been attributed [23,24] to dielectronic satellite transitions originating from collisionally redistributed $1s2l3l'$ Li-like levels. We note that the blue wing emission duration is fairly short (≈ 4 ps) and that a similar wing appears on the blue side of the He_β line around 6.59 Å.

IV. DATA ANALYSIS AND RESULTS

We use the observed relative intensity of the resonance lines to the associated satellites, e.g., see Fig. 3, to obtain a physical picture of the initial phase of the laser heating. We first analyze the spectral data with a simple atomic physics model based on a calculation of the number and volume of the emitting ions. The fact that at early time the plasma has not yet undergone significant hydrodynamic expansion so that the ions remain at solid density provides a starting point for the analysis. By estimating the relative intensity of the satellite to line emission, we can obtain the relative number of ions emitting satellites to the number emitting resonance lines, and, employing the experimental intensity ratio, find the volume of emitting material. This calculation provides the foundation for the interpretation that the initial energy deposition creates a large volume, low temperature plasma surrounding the hot laser-spot plasma.

To calculate the intensity distribution between the resonance lines and the associated satellites, we consider the ratio of the He_β line to the satellites that are well separated from it. This means that we include the transitions $(1s)(2s2p)(4s4p4d4f)\rightarrow(1s)^2\ (2s2p)$—we use the superconfiguration notation, see below—but not the transitions $(1s)(3s3p3d)(4s4p4d4f)\rightarrow(1s)^2\ (3s3p3d)$, which are very close to the resonance line. The satellite to He_β resonance line intensity ratio observed in the first 500 fs can be measured to be 0.2 in Fig. 3 (see thin solid line). The states that give rise to the satellites from the $(1s)(2s2p)(4s4p4d4f)\rightarrow(1s)^2\ (2s2p)$ configuration cannot exist in a high temperature (i.e., T must be less than ≈ 200 eV) plasma. On the other hand, the He_β transition can not exist in a low temperature (i.e., T must be greater than ≈ 500 eV) plasma. Thus we have only one possible explanation and that is the two emission signals arise from different temperature regions. The situation at a later time, on the picosecond time scale, is well described by a single temperature and line radiation is observed to dominate, implying that a uniform density plasma is attained only after hydrodynamic expansion.

To find the volume ratio V between the two initial plasmas, i.e., the hot laser spot and the surrounding low temperature volume heated by hot electrons, we calculate the intensity ratio between resonance and satellite emission, assuming solid density. We choose 150 eV as the temperature of the low temperature plasma, as this maximizes the number of ions that emit He satellites when we determine the ion populations using the collisional-radiative model described below.

The temperature of the hot laser spot is taken to be 1.7 keV, the temperature that best fits a simple simulation of the resonance line time history using a hydrodynamic foil expansion coupled with a time-dependent atomic population kinetics model physics analysis. This simulation will be described in detail later in this section. We note that using 1.5 or 2.0 keV does not effect the time history of the resonance line, in any manner that would modify the physical picture of the heating mechanism. With these values, we equate the calculated emission ratio to the observed ratio:

$$[VI_s(150)+I_s(1700)]/[VI_r(150)+I_r(1700)]=0.2, \quad (1)$$

where $I_s(T)$ and $I_r(T)$ are the intensity of the satellite and resonance line emissions at temperature T, respectively and 0.2 is the observed intensity ratio. At 1.7 keV the local thermodynamic equilibrium (LTE) number density of the $(1s)\times(3s3p)$ ions emitting He_β is 0.14×10^{20} cm^{-3} and the number density of the satellite emitters $(1s)(2s2p)\times(4s4p4d4f)$ is 0.81×10^{17} cm^{-3}. The radiative decay rate value for He_β is 4.84×10^{11} s^{-1} and for the $n=4$ satellites is 1.6×10^{11} s^{-1}, where the statistical weight 512 has been included. We note that for these assumed conditions the satellite to line intensity ratio $I_s(1700)/I_r(1700)=1.9\times10^{-3}$, so that as expected, the high temperature plasma has little satellite emission. In LTE, at 150 eV, the number density of the upper manifold of He_β is 0.39×10^{18} cm^{-3}, and the number density of the manifold of $n=4$ satellites is 0.55×10^{18} cm^{-3}. Thus, we have $I_s(150)/I_r(150)=0.46$ and significant satellite emission is found for this plasma. Substituting into Eq. (1), we find that V, the ratio of volume of the two plasmas, is 27, and since the depth of the two plasmas is the same, the plasmas occupy areas with radii having a ratio of 5. This straightforward calculation shows that the initial (<500 fs) emitted spectrum is consistent with a two-plasma model. A plasma with an area large compared to the laser spot is heated to a low temperature (150 eV), while the smaller laser spot has a higher temperature (1.7 keV).

Initially, the electrons in the laser spot are accelerated by the strong laser radiation field to a high energy, the laser quiver energy is ≈150 keV for the maximum laser irradiance used. These high energy electrons experience few collisions when they are in the field of the laser. Indeed, their mean free path is large compared to the foil thickness, so that they spread over a surface much larger than the initial focal spot and lose their energy in a few hundred femtoseconds to multiply excited ions and thermal electrons, creating a large area, low temperature plasma. This is the primary mechanism for the initial transverse spatial heat transfer. The flow of these hot electrons produces a charge separation because of the larger mass of the ions, resulting in a large electrostatic field. This potential energy is damped by the acceleration of ions out of the solid target, which also can be shown to take place on a time scale of several hundred femtoseconds [25–27]. The inward flow of hot electrons returning to the target after being expelled is compensated by a counterstreaming flow of cold electrons from the target which neutralizes the hot electron flow. This is a mechanism that acts over a large area of the foil, and is an additional factor in the nonuniform radial distribution of electron temperature. The hot laser spot, which has a temperature of a few keV, emits primarily resonance radiation. At a later time, hydrodynamic cooling means that the emission from the laser spot will dominate.

To perform a more detailed analysis of the initial heating phase, we first note that scaling laws for the characteristic plasma parameter lengths have been obtained from a self-consistent analytical model of the anomalous and normal skin effects in plasmas with a step density profile [28]. Results show that for pulse durations ≈100 fs, the skin depth is larger than the displacement of the critical density surface up to an intensity of 10^{17} W μm^2/cm^2. Above this irradiance, the laser pulse interacts with an expanding plasma of finite electron density gradient scalelength. The one-dimensional (1D) particle-in-cell (PIC) simulations performed by Lawson and his collaborators [29] for generic conditions of 100 nm foils irradiated by 100 fs pulses at relativistic intensities are of interest in confirming the heating model presented above. These calculations show [30,31] that, for the laser irradiance used in our experiment, a large fraction of the absorbed laser energy (about 10%) does indeed produce the electrons at the laser quiver energy that are responsible for heating a broad area of the foil and for creating the conditions that favor satellite line emission. This is also confirmed experimentally by the data from the hard x-ray scintillator (diode) array that show that a large fraction of the absorbed laser energy is transferred to electrons at the laser field quiver energy. Simulations performed for slightly thicker foils (>100 nm) using a 2D PIC code also show that the high energy electrons spread over a surface larger than the initial focal spot [22] with a return current compensated by a cold electron current counterpart that neutralizes the hot electron flow.

In the initial phase, most of the fast electron energy is transferred to the ions and electrons in the large area, low temperature plasma. However, the average electron energy remains on the order of tens of keV [25] and the electron density is still quite high. To estimate the thermalization time for the hot electrons created in the laser spot after the fast electrons have been created, it is important to have an accurate description of their energy budget. We thus investigate the processes by which the electrons with energies above 100 keV are degraded to a few hundred eV, where multiply excited ions become the most important species and satellite lines dominate the emission. The hot electrons thermalize with the cold electron backgound on the time scale given by the equilibration time for two-temperature electron distributions [32]:

$$\tau_{ee}\approx(1.7\times10^5/n_e\lambda_{ee})(T_{\rm hot}+T_e)^{3/2}, \quad (2)$$

where λ_{ee} is the Coulomb logarithm. For $n_e=10^{23}$ cm^{-3}, assuming a bulk temperature of 500 eV, and with a hot electron temperature of 10 keV, Eq. (2) yields a relaxation time of ≈250 fs. Thus, after a few hundred femtoseconds the electron distribution function becomes Maxwellian. The 1D PIC calculations incorporating collisions [25] confirm this relaxation time and show also that the characteristic temperature decreases very rapidly. In fact, the data displayed in Fig.

4 show shorter resonance line emission durations for thicker foils. The thicker the foil, the smaller is the amount of hydrodynamically expanded matter relative to the bulk.

To obtain detailed information on laser plasma emission, an investigation using hydrodynamic simulations postprocessed by a collisional-radiative model [33] is usually performed. This analysis is not possible for the present short-pulse high-intensity experimental conditions because the fluid description of hydrodynamics codes fails for this case. As shown by PIC simulations, the ponderomotive pressure of the laser light in this experiment is much higher than the thermal pressure. However, because we expect quite uniform temperature and density conditions in the direction perpendicular to the target surface even for times larger than 500 fs after laser peak, we can follow the expansion of the foil with a 1D hydrocode, FILM [34]. Because we cannot couple the laser radiation field to the electrons in the foil, an initial condition —the value of the temperature of the laser spot in the longitudinal direction— is introduced. This arbitrary initial foil temperature is a variable parameter, determined in these simulations to obtain the best agreement with experiment. The time resolved spectra are calculated using TRANSPEC [16] as a postprocessor. TRANSPEC is a 1D planar, radiation dependent, collisional-radiative spectroscopy code. The basic version models time-dependent *K*-shell emission and can act as a postprocessor for any plasma hydrodynamics simulation. The radiation is coupled self-consistently with the populations in an iterative procedure. The populations are obtained by linearization and line transfer is computed within the core saturation approximation. In simulations of the time-dependent populations of Al plasma ions, only line transfer of the resonance lines He_α, He_β, and H_α, H_β has been taken into account, since all other lines are optically thin. For the treatment of bi-Maxwellian electron distributions, the model can also handle two different electronic temperatures, at one ion temperature. A fast and accurate in-line routine that calculates H-like and He-like Stark profiles has been added for the simulations performed here.

Because satellite lines contribute a large intensity to the emission, a great number of levels were required to model the spectrum, resulting in an extremely large population matrix in the collisional-radiative model. To reduce the size of this matrix, superconfiguration accounting was performed for all the ions from Al I to Al XI. This drastically reduces the total number of detailed levels and the number of configurations incorporated in the collisional-radiative population model. We included superconfigurations with quantum numbers up to $n=5$ and superconfigurations with a vacancy in the $1s$ shell in the accounting for the ions treated in our simulations. As an example, we show in Table I a list of the superconfigurations used in the model for the Li-like ion. Next, the AVERROES [17] code was used to calculate the collisional and radiative rates as well as the mean energies and variances of all the possible electron radiative transitions. Finally, these quantities were stored and TRANSPEC was used to calculate the time-dependent populations, the emissivity, and the opacity of the plasma.

It is well known that the creation of suprathermal electrons during the laser pulse can lead to a distortion of the nominal ionization balance by the inner-shell ionization process. It has been shown [11,35] that this affects mainly the H-like fraction as compared to the lower charge states. However, for the very high density plasma created here, where the hot electrons lose their energy primarily by ion acceleration due to laser-induced electron-ion charge separation, the ionization balance rapidly settles to a steady state. To verify that the steady state ionization balance is attained, we performed collisional-radiative calculations incorporating inner-shell ionization, with the result that the ionization due to a burst of fast electrons does not change the average charge state. We performed further simulations with a 500 fs burst of 10–100 keV electrons, where the hot electron energy content was assumed to be 8% of the laser energy. These additional electron bursts did not change the spectral shape of the He_β and He_γ transitions nor the features in the spectral region between them.

TABLE I. Partial list of superconfigurations used for the Li-like stage of aluminum.

Name	Energy (eV)	Degeneracy
$(1s)^2\ (2s2p)$	0	8
$(1s)^2\ (3s3p3d)$	240	18
$(1s)^2\ (4s4p4d4f)$	322	32
$(1s)^2\ (5s5p5d5f5g)$	359	50
$(1s)(2s2p)^2$	1568	56
$(1s)(2s2p)(3s3p3d)$	1825	288
$(1s)(2s2p)(4s4p4d4f)$	1908	512
$(1s)(2s2p)(5s5p5d5f5g)$	1946	800
$(1s)(3s3p3d)^2$	2097	306
$(1s)(3s3p3d)(4s4p4d4f)$	2186	1152
$(1s)(3s3p3d)(5s5p5d5f5g)$	2225	1800
$(1s)(4s4p4d4f)^2$	2279	992
$(1s)(4s4p4d4f)(5s5p5d5f5g)$	2320	3200
$(1s)(5s5p5d5f5g)^2$	2362	2450

The accuracy of TRANSPEC was checked for several density and temperature combinations with HULLAC [36], a detailed atomic physics code. To verify that the superconfiguration accounting provides a representation of more detailed calculations of emission, a HULLAC calculation was performed with 3553 levels. The 3553-level HULLAC model is compared to the 140-superconfiguration-level combinations employed in TRANSPEC (AVERROES) in Fig. 5 for a steady case. There is good qualitative agreement between the two codes, and we can evaluate the accuracy of the TRANSPEC (AVERROES) approximation compared to the more detailed HULLAC model.

In Fig. 6 we display the experimental and FILM simulation histories of the He_β and He_γ lines obtained from a 50 nm and 75 nm foil heated to 1700 eV and 1200 eV, respectively. The data is convolved with a 2-ps FWHM Gaussian to take into account the finite time resolution of the spectrometer coupled to the streak camera. The main features of the time-resolved spectra are reproduced quite accurately. We note that this determination is sensitive to the maximum foil temperature.

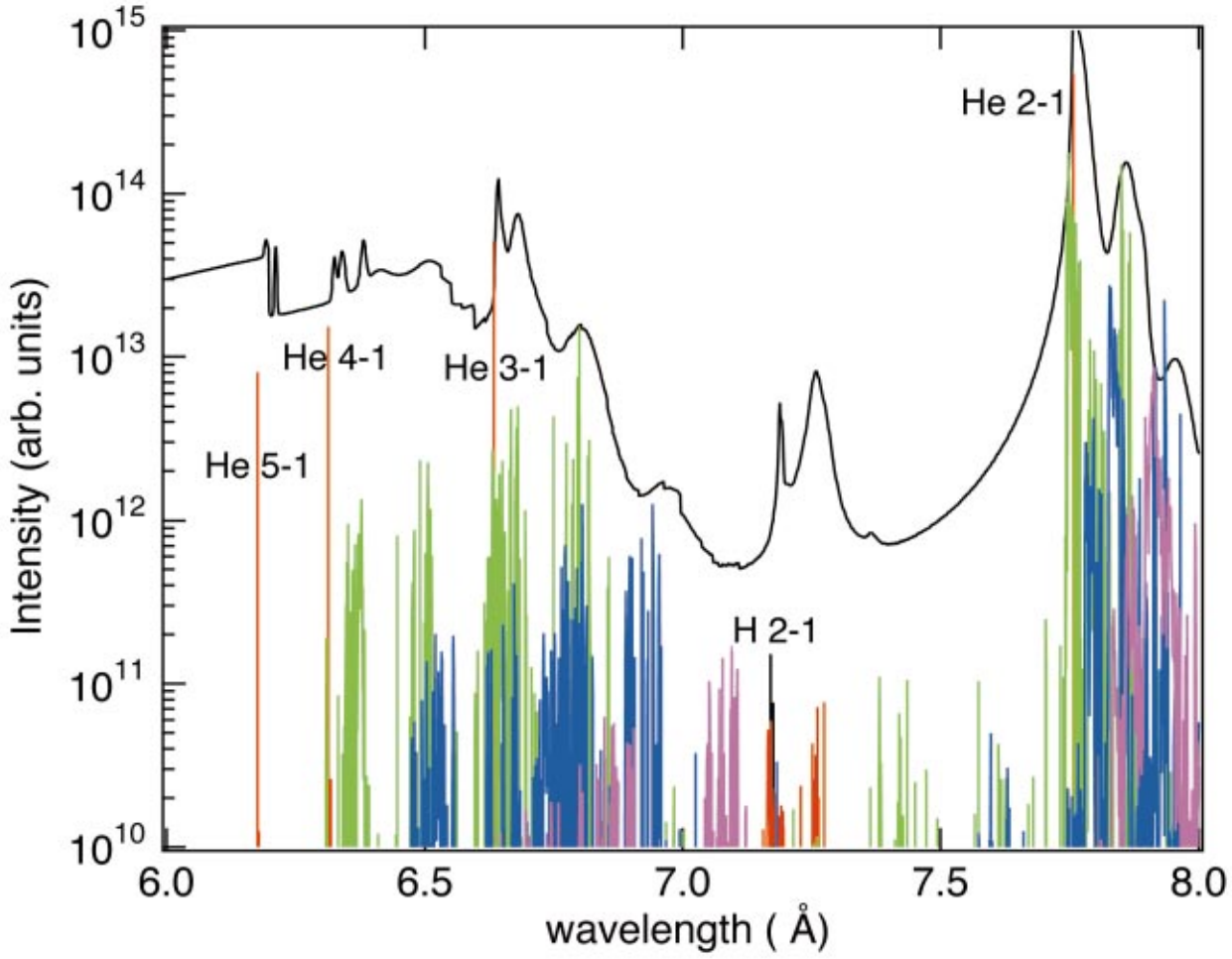

FIG. 5. (Color) Theoretical spectra of the He_α–$He\delta$ wavelength regions and two-electron satellites. The electron temperature is 200 eV and the electron density is 10^{23} cm^{-3}. Vertical bars denote individual transitions calculated by HULLAC (black, H-like lines; red, He-like lines; green, Li-like lines, blue, Be-like lines; pink, B-like lines). The solid black line is the TRANSPEC result.

For example, if the temperature is lowered to 500 eV or raised to 5 keV, no agreement could be obtained [see Figs. 6(a) and 6(b)].

Since we assert that the satellite lines from ions less charged than Al XI play a significant role in the early time spectra observed for the range of densities and temperatures in the present experiment, we have calculated the spectra originating from the high-lying ($n \geqslant 3$) doubly excited levels in order to illustrate their importance. In Fig. 7 we compare TRANSPEC spectra calculated with and without the satellites from ionization stages lower than Li-like (Li-like and He-like satellites are treated as individual lines in TRANSPEC). Without the high-n satellite transitions, several important line features that clearly are observed to fill the spectral region between the He_γ and He_β resonance line transitions are missing in the spectrum. The missing features are identified as the Be-like satellites around 8 Å, the satellites of He_β around 6.8 Å, and the $n=4$ satellites around 6.5 Å.

We show in Fig. 8 a comparison of the simulation to the traces of the spectral region between the He_β and He_γ resonance lines as a function of time. The simulations have been scaled to match the experiment. We can see that the detailed features of the $n=4$ satellites are not well reproduced for a number of reasons. First, the averaging process inherent in the superconfiguration approach does not permit the detailed reproduction of small-scale spectral features. Second, the calculation of the reabsorption was performed using the statistical width for the superconfiguration instead of the individual Stark-broadened linewidths. Third, and finally, we have assumed a 1D expansion with a homogeneous density over the entire focal spot.

V. SUMMARY AND CONCLUSIONS

We have performed a spectroscopic analysis of the *K*-shell emission from relativistic aluminum plasmas created from ultrathin foils heated with a high-intensity, high contrast, ultrashort-pulse laser. The small foil thickness in this experiment minimized thermal gradients in the longitudinal direction and allowed a simple physical interpretation of the spectral data. We found that when such a foil is heated with a short laser pulse, the laser accelerates fast electrons that, through space charge separation, rapidly transfer their energy to ions with multiply excited levels and core vacancies that emit a broad satellite spectrum. The associated return currents contain colder electrons, and accordingly a large area of

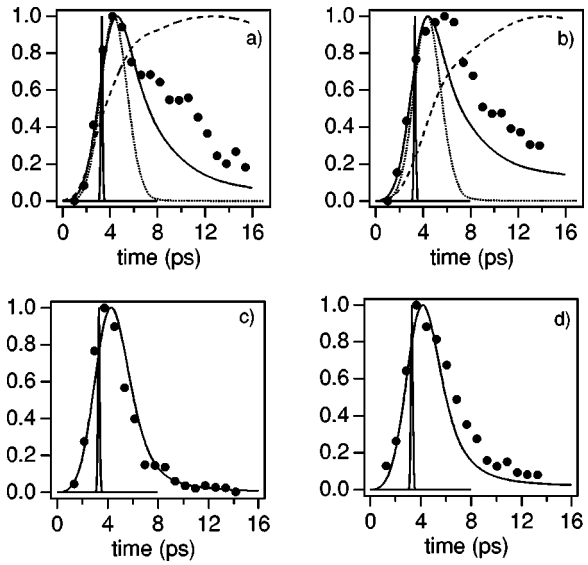

FIG. 6. Time-resolved spectra of He_γ [(a) and (c)] and He_β [(b) and (d)] for a 50-nm [(a) and (b)] and a 75-nm [(c) and (d)] foil. Laser pulse duration is 150 fs and laser intensity is 2×10^{19} W/cm^2. The dots are the experimental data. The temporal position of the laser pulse is indicated but the time origin is different from that in Figs. 2 and 4. Solid lines give the simulation for a temperature of 1700 eV [(a) and (b)] and 1200 eV [(c) and (d)]. For the 50-nm case [(a) and (b)], simulations results for 500 eV (dotted line) and 5000 eV (dashed line) are also shown. Simulation and experimental results are scaled to the maximum of the experimental intensity.

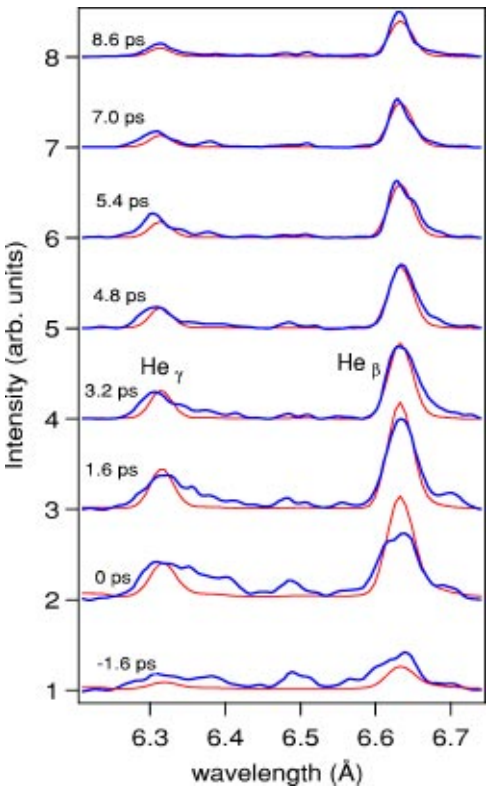

FIG. 8. (Color) Time-resolved spectra of He_γ and He_β lines for a 50-nm foil at 2×10^{19} W/cm^2 laser irradiance. Experiment (heavy line) and theory (thin line). For each time, curves are displaced vertically by one unit.

the foil (compared to the laser spot) rapidly attains a uniform and quite low temperature $\approx$100 eV. The near solid density plasma in the laser spot is found to have an initial temperature $\approx$ 1 keV. This sequence of events is reflected in the initial time-resolved spectrum recorded in the first 500 fs after initial target emission, which displays intense satellites along with the He-like resonance lines. This spectrum has been successfully interpreted using a simple hydrodynamic expansion model for the laser-spot heating in tandem with TRANSPEC (AVERROES) to determine by best fit to the observed spectrum, an initial temperature of 1.7 keV for the 50 nm-foil. An assumed initial temperature in the laser spot of 1.2 keV was required for the 75-nm foil. With these values for the laser-spot temperature, a second plasma temperature is required to account for the intense satellite emission This second plasma was shown to have an area 25 times the laser spot area and a temperature of 150 eV. These plasmas subsequently cool primarily by hydrodynamic expansion and the resonance line radiation from the hot laser spot dominates at later time, so that in the time-integrated spectrum the satellite contribution is barely discernable.

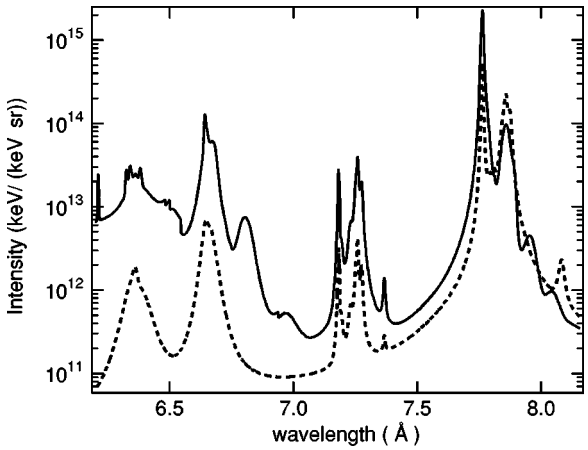

FIG. 7. TRANSPEC spectra at 250 eV electron temperature and 3×10^{22} cm^{-3} ion density including (solid line) or excluding (dashed line) satellites originating from the high-lying ($n\geqslant3$) doubly excited levels of ions less charged than Li-like aluminum.

The atomic physics of very high intensity ($I\lambda^2\geqslant2\times10^{18}$ W μm^2/cm^2) laser solid interaction is far from being fully understood. Nevertheless, the importance of satellite transitions from doubly excited levels in low-charged ions has been evidenced here. Our work has important implications for the study of the influence of non-Maxwellian distribution functions on the population dynamics of multicharged ions. We also have shown the usefulness of the nonlocal thermal equilibrium superconfiguration approach, which accounts for the overwhelming multiplicity of the excited levels of multicharged ions, in the collisional-radiative modeling of hot, dense, and highly transient plasmas. The recorded spectra were compared to simulations involving simple hydrodynamics, level populations, line intensities, and spectral shapes calculated by a collisional-radiative

model using the superconfiguration approximation. The result of this comparison confirms that there is a problem associated with spectral diagnostics that are based solely on time-integrated spectra. It also reinforces the conclusion that because of the important role of doubly excited states in the formation of the dominant spectral features at early time with near-solid plasma densities, the complex interplay of the thermal and nonthermal electron distributions in the population of singly and multiply excited states must be understood. In addition, some drawbacks in the study of high intensity laser-irradiated thin foils, such as radial inhomogeneities, are identified. The spatial resolution of the streak camera in this experiment is larger than the laser focal spot, since it is defined by the 100 μm entrance slit. Since the x-ray instrumentation did not provide spatially resolved data, the conclusion that a large area, cool plasma is created initially was found by deduction from a heating model. Spatially resolved data could be acquired using a dot target. The possibility of producing a high density, hot plasma by a very short pulse, high-intensity laser requires further study.

ACKNOWLEDGMENTS

The authors would like to thank Jean-Paul Geindre for numerous and helpful discussions. We acknowledge the invaluable support of the USP technical staff at LLNL. This work was performed under the auspices of the U.S. DOE by the University of California, LLNL under Contract No. W-7405-Eng-48. Partial support was also provided by DOE HEDS Grant No. DE-FG03-98DP00213 to Howard University.

[1] P. Gibbon and E. Förster, Plasma Phys. Controlled Fusion **38**, 769 (1966).
[2] P. Audebert, J.-P. Geindre, A. Rousse, F. Falliès, J.-C. Gauthier, A. Mysyrowicz, G. Grillon, and A. Antonetti, J. Phys. B **27**, 3303 (1994).
[3] J.-C. Gauthier, J.-P. Geindre, P. Audebert, S. Bastiani, C. Quoix, G. Grillon, A. Mysyrowicz, A. Antonetti, and R. Mancini, Phys. Plasmas **4**, 1811 (1997).
[4] D. Altenbernd, U. Teubner, P. Gibbon, E. Förster, P. Audebert, J.-P. Geindre, J.-C. Gauthier, G. Grillon, and A. Antonetti, J. Phys. B **30**, 3969 (1997).
[5] J.-C. Kieffer, Z. Jiang, A. Ikhlef, C. Côté, and O. Peyrusse, J. Opt. Soc. Am. B **13**, 133 (1996).
[6] C.Y. Côté, J.-C. Kieffer, Z. Jiang, A. Ikhlef, and H. Pépin, J. Phys. B **31**, L883 (1998).
[7] A. Saemann, K. Eidmann, I.E. Golovkin, R. Mancini, E. Anderson, E. Förster, and K. Witte, Phys. Rev. Lett. **82**, 4843 (1999).
[8] K. Eidmann, A. Saemann, U. Andiel, I. Golovkin, R. Mancini, E. Anderson, and E. Förster, J. Quant. Spectrosc. Radiat. Transf. **65**, 173 (2000).
[9] U. Andiel, K. Eidmann, and K. Witte, Phys. Rev. E **63**, 026407 (2001).
[10] J.-P. Matte *et al.*, Phys. Rev. Lett. **72**, 1208 (1994).
[11] F.B. Rosmej, J. Phys. B **30**, L819 (1997).
[12] C.Y. Côté, J.-C. Kieffer, and O. Peyrusse, Phys. Rev. E **56**, 992 (1997).
[13] R. Shepherd, R. More, B. Young, D. Price, R. Walling, A. Osterheld, R. Stewart, and T. Kato, J. Quant. Spectrosc. Radiat. Transf. **58**, 911 (1997).
[14] P. Gallant, Z. Jiang, C. Chien, P. Forget, F. Dorchies, J.-C. Kieffer, H. Pépin, O. Peyrusse, G. Mourou, and A. Krol, J. Quant. Spectrosc. Radiat. Transf. **65**, 243 (1999).
[15] K. Eidmann *et al.*, in *Atomic Processes in Plasmas*, edited by R. Mancini and R. Phaneuf, AIP Conf. Proc. No. 547 (AIP, New York, 2000), pp. 238–251.
[16] O. Peyrusse, Phys. Fluids B **4**, 2007 (1992); J. Quant. Spectrosc. Radiat. Transf. **51**, 281 (1994).
[17] O. Peyrusse, J. Phys. B **32**, 683 (1999); **33**, 4303 (2000).
[18] W. White, J. Hunter, L. van Woerkom, T. Ditmire, and M. Perry, Opt. Lett. **17**, 1069 (1992); A. Sullivan, J. Bonlie, D.F. Price, and W.E. White, Opt. Lett. **21**, 603 (1996).
[19] D.J. Kane and R. Trebino, IEEE J. Quantum Electron. **29**, 571 (1993).
[20] B.J. MacGowan, Rutherford Appleton Report RL-82-039, 1982 (unpublished).
[21] A. Yamaguchi and J. Nizui, Phys. Lett. **72A**, 333 (1979).
[22] J. Fuchs, J.-C. Adam, F. Amiranoff, S. Baton, N. Blanchot, P. Gallant, L. Gremillet, A. Héron, J.-C. Kieffer, G. Laval, G. Malka, J. Miquel, P. Mora, H. Pépin, and C. Rousseaux, Phys. Plasmas **6**, 2569 (1999).
[23] F.B. Rosmej, B. Bryunetkin, A.Ya. Faenov, I.Yu. Skobelev, M. Kalashnikov, P. Nickles, and M. Schnürer, J. Phys. B **29**, L299 (1996).
[24] F.B. Rosmej and J. Abdallah, Jr., Phys. Lett. A **245**, 8176 (1998).
[25] S. Weber, G. Bonnaud, and J.-C. Gauthier, Phys. Plasmas **8**, 387 (2001).
[26] Y. Sentoku, K. Mima, T. Taguchi, S. Miyamoto, and Y. Kishimoto, Phys. Plasmas **5**, 4366 (1998).
[27] Y. Sentoku, T. Liseikina, T. Esirkepov, F. Califano, N. Naumova, Y. Ueshima, V. Vshivkov, Y. Kato, K. Mima, K. Nishihara, F. Pegoraro, and S. Bulanov, Phys. Rev. E **62**, 7271 (2000).
[28] W. Rozmus and V. Tikhonchuk, Phys. Rev. A **42**, 7401 (1990).
[29] W.S. Lawson, P.W. Rambo, and D.J. Larson, Phys. Plasmas **4**, 788 (1997).
[30] G. Malka, E. Lefebvre, and J.-L. Miquel, Phys. Rev. Lett. **78**, 3314 (1997).
[31] A. Zhidkov and A. Sasaki, Phys. Plasmas **7**, 1341 (2000).
[32] D. Book, *NRL Plasma Formulary* (Naval Research Laboratory, Washington, D.C. 1990).
[33] K. Eidmann, J. Meyer-ter-Vehn, T. Schlegel, and S. Hüller, Phys. Rev. E **62**, 1202 (2000).
[34] U. Teubner, P. Gibbon, E. Förster, F. Falliès, P. Audebert, J.-P. Geindre, and J.-C. Gauthier, Phys. Plasmas **3**, 2679 (1996).
[35] F. Rosmej *et al.*, J. Quant. Spectrosc. Radiat. Transf. **65**, 477 (2000).
[36] A. Bar-Shalom, M. Klapisch, and J. Oreg, J. Quant. Spectrosc. Radiat. Transf. **71**, 169 (2001).